Materials Characterization 106 (2015) 266–272

Contents lists available at ScienceDirect

Materials Characterization

journal homepage: www.elsevier.com/locate/matchar

Microstructural evolution and creep-rupture life estimation of high-Cr martensitic heat-resistant steels

Kyu-Ho Lee [a], Jin-Yoo Suh [b], Sung-Min Hong [b], Joo-Youl Huh [c], Woo-Sang Jung [b,*]

[a] Special Steel Development Team, Hyundai Steel, Chungnam 343-823, Republic of Korea
[b] High Temperature Energy Materials Research Center, Korea Institute of Science and Technology, Seoul 136-791, Republic of Korea
[c] Department of Materials Science and Engineering, Korea University, Seoul 136-713, Republic of Korea

ARTICLE INFO

Article history:
Received 13 February 2015
Received in revised form 2 June 2015
Accepted 7 June 2015
Available online 10 June 2015

Keywords:
Heat-resistant steels
Precipitation
Z-phase
Creep-rupture life
Monkman–Grant equation

ABSTRACT

The creep behavior of high-Cr martensitic heat-resistant steels was investigated to discuss the dominant factors determining the creep-rupture life in the temperature range from 839 to 894 K. Variation in the content of Nb, a carbide former, induced a difference in creep-degradation at the long-term creep condition, which was attributed to the formation of a Z-phase at the expense of M_2N precipitates. Due to the continuous evolution of the microstructure during creep service, a simple form of the Monkman–Grant equation could not properly describe the creep-rupture life of the alloys; however, the modified Monkman–Grant equation, which incorporates the creep rate at the tertiary creep region, resulted in a reasonable estimation of creep-rupture life.

1. Introduction

9–12% Cr martensitic heat-resistant steel is characterized by its superior resistance to oxidation, corrosion, and creep deformation. In addition, the steels are characterized by superior thermo-fatigue resistance compared to that of austenitic heat-resistant steel and a low thermal expansion coefficient. For these reasons, the 9–12% Cr martensitic heat-resistant steels have been constituting the critical parts withstanding hot pressurized steams in the boiler unit of current coal-fired power plants [1–3]. These days, we are facing a significant threat to human society imposed by the limited natural resources and the surge of greenhouse gas emission. To cope with the current situation, not only the development of novel energy resources but also the increase in the efficiency of current power generation, such as coal-fired power generation, is highly required. A foremost requirement for improving power generation efficiency in coal-fired power plants is to increase the operating temperature and steam pressure [3–5]. Thus, the development of materials that can be used in higher temperatures and pressure conditions for a longer time is demanded. As a result, research and development on heat-resistant steel with a superior high-temperature creep property is actively underway [1–8]. An efficient method that improves high-temperature creep properties is to utilize precipitation strengthening. In this context, a number of studies have been conducted on the formation of MX (M = Ti, V, Nb, Ta etc./X = C, N) carbonitride, which is stable at high-temperatures, by adding transition elements such as Ti, V, Nb, and Ta [8]. For the requirements a candidate heat-resistant steel has to meet, ASME Section II defines the following standards regarding the allowable stress values of coal-fired power plants below 1088 K: (1) 100% of the average stress to produce a creep rate of 0.01% in 1000 h ($=10^{-5}$%/h), and (2) 80% of the minimum stress and 67% of average stress to cause rupture at 100,000 h [9]. However, it is not practical to perform a creep test for about 11.4 years (100,000 h). Thus, the traditional estimation of creep strength at 100,000 h has been done by extrapolating from experimental results of less than 30,000 h by making various temperature and stress conditions [7]. Typical estimation methods of creep-rupture life include, (1) a Larson–Miller plot [10,11] based on variables of time and temperature, and (2) a Monkman–Grant plot [12], in which creep-rupture life does not correlate with temperature but is inversely proportional to

Table 1
Chemical composition of high-Cr martensitic heat-resistant steels used in this study (wt.%).

Alloy	Fe	C	Si	Mn	Ni	Cr	Mo	V	W	Cu	Nb	N
Steel A	Bal.	0.18	0.23	0.69	0.52	10.9	0.98	0.20	0.16	0.03	0.06	0.072
Steel B	Bal.	0.16	0.25	0.56	0.35	10.4	0.86	0.17	–	0.13	0.38	0.061

* Corresponding author.
E-mail addresses: kyuhos@hyundai-steel.com (K.-H. Lee), jinyoo@kist.re.kr (J.-Y. Suh), magerit84@gmail.com (S.-M. Hong), jyhuh@korea.ac.kr (J.-Y. Huh), wsjung@kist.re.kr (W.-S. Jung).

http://dx.doi.org/10.1016/j.matchar.2015.06.005
1044-5803/

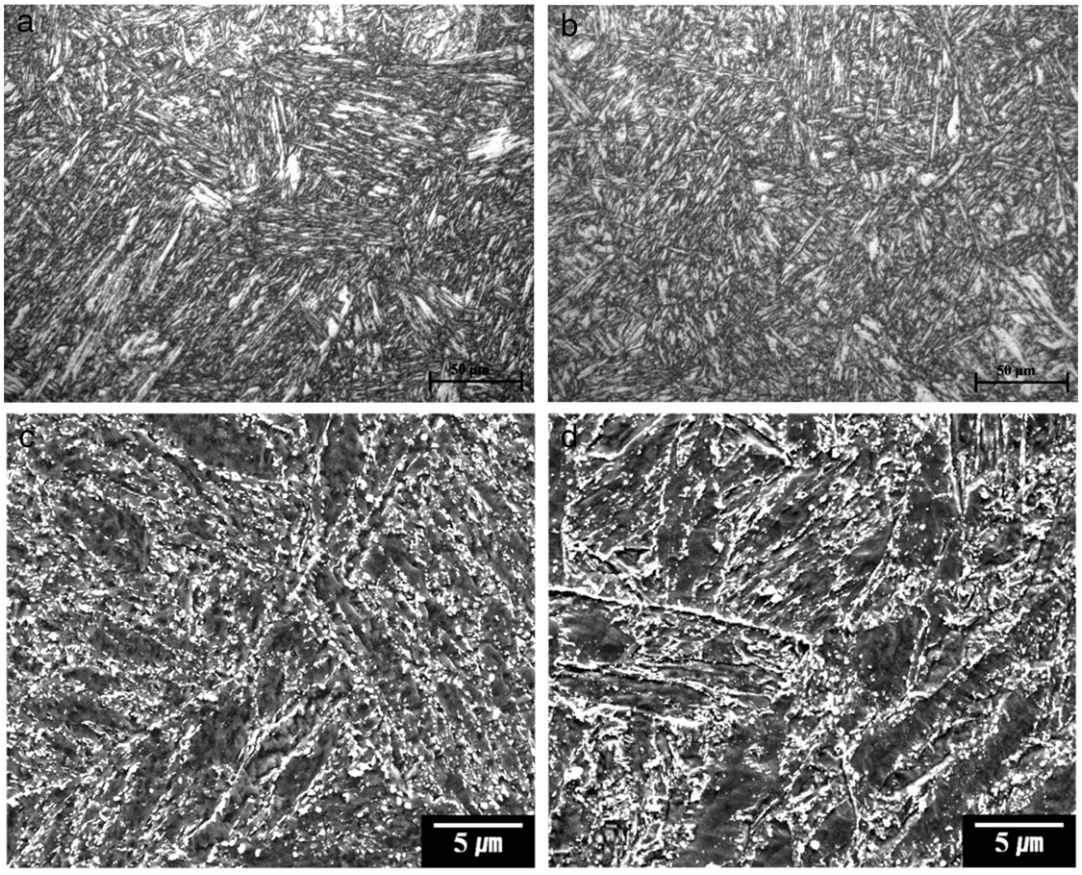

Fig. 1. OM and SEM micrographs of both steels, observed after tempering. OM image of (a) Steel A and (b) Steel B. SEM image of (c) Steel A and (d) Steel B (before creep tests).

the minimum creep rate ($\dot{\varepsilon}_{min}$). They have long been used to estimate the creep-rupture life of many different heat-resistant metals, however it was also reported that the equations were no longer reliable in case of continuous microstructural evolution such as secondary precipitation, coarsening of precipitates, and recrystallization during long-term creep service [13]. Therefore, this study aimed to evaluate the validities of different model equations using the long-term creep data of high-Cr martensitic heat-resistant steels which turned out to have a significant change in creep behavior during long-term creep exposure due to the microstructural evolution. The high-Cr steels were designed to have a different Nb content, which is a strong MX-forming element, to induce a different microstructural evolution among the alloys during creep deformation. Careful observation of the microstructures was carried out to explain the change in creep deformation behavior. Also the creep-rupture life estimated by the model equations was compared with the experimental data.

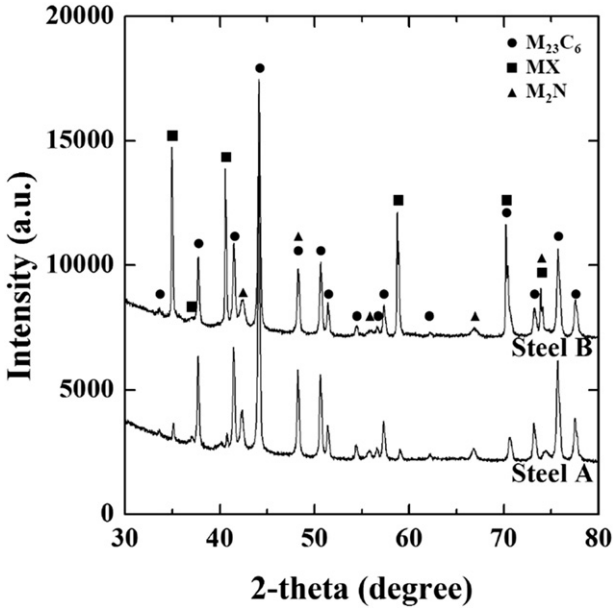

Fig. 2. XRD profiles of the powder electrochemically extracted from Steel A and Steel B after tempering (before creep test).

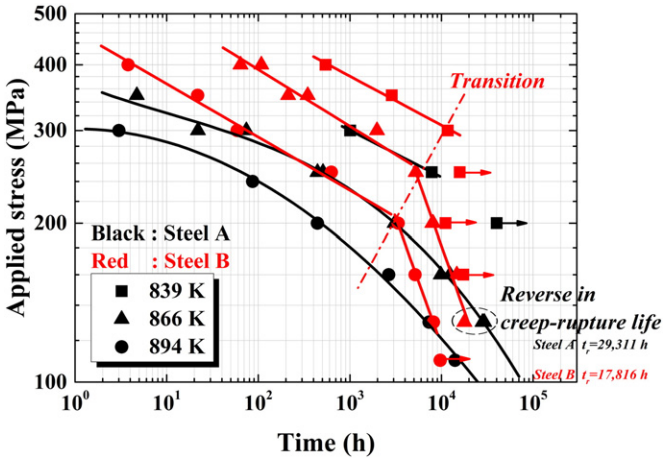

Fig. 3. Creep-rupture properties of Steel A (black symbol) and Steel B (red symbol) acquired through various creep test conditions (the arrow indicates that the creep test for both steels is still ongoing).

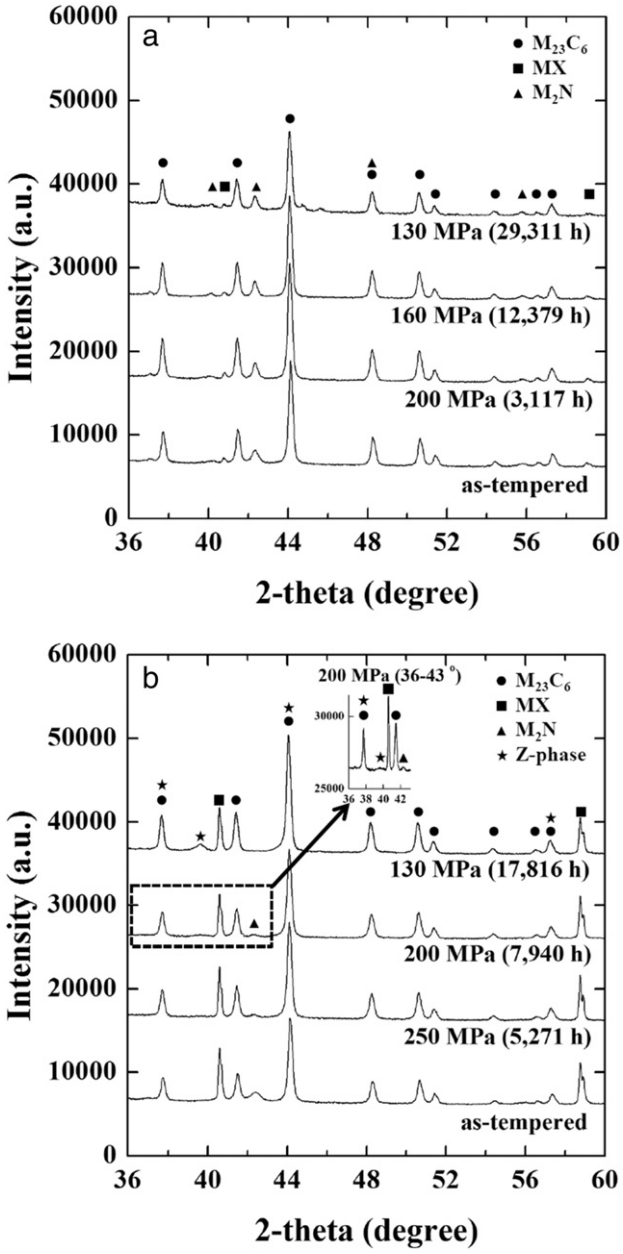

Fig. 4. XRD diffraction profiles of the powder electrochemically extracted from the gauge part of creep-ruptured specimens of (a) Steel A and (b) Steel B at 866 K.

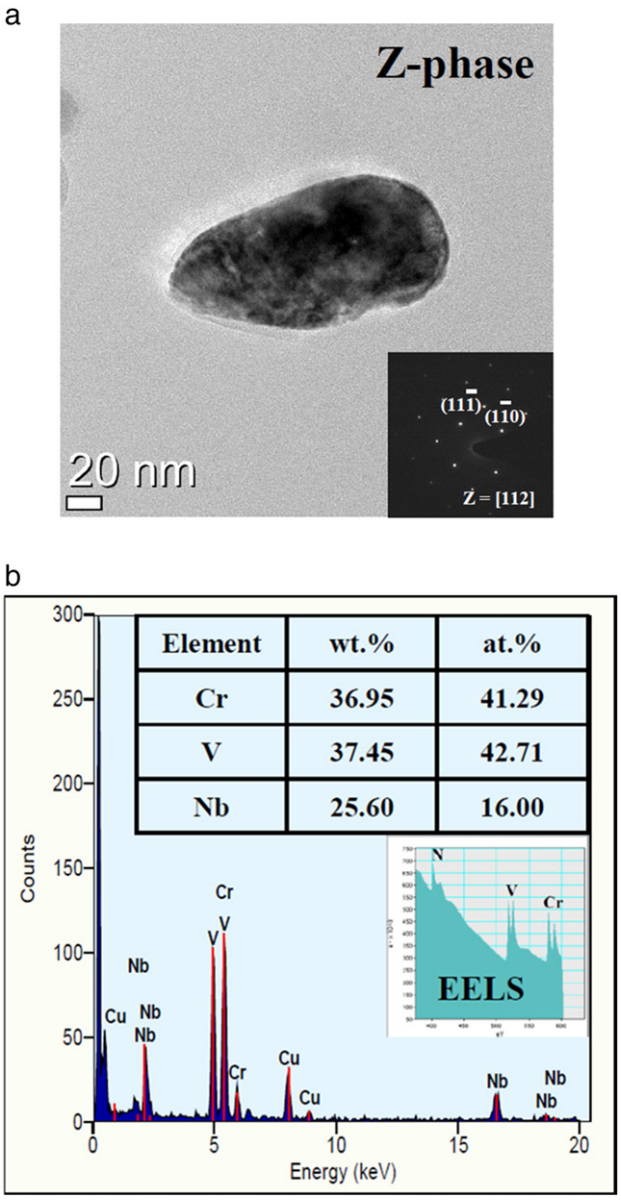

Fig. 5. TEM micrographs of Steel B creep-ruptured at 866 K under 130 MPa ($t_r = 17{,}816$ h). (a) Bright-field image and SAED pattern, and (b) EDS analysis and EELS spectrum.

2. Experimental procedure

The chemical composition of the high-Cr martensitic heat-resistant steels used in this study is shown in Table 1. The steels were provided by Doosan Heavy Industries & Construction Co., Ltd. Steel A has a typical composition of high-Cr martensitic heat-resistant steels. Steel B has almost the same chemical composition as that of Steel A with a difference in the content of Nb. The following heat-treatment process was conducted to make the prior austenite grain (PAG) size of the two steels similar (50–60 μm). Steel A and Steel B were normalized at temperatures of 1323 and 1373 K, respectively, and subsequently tempered at 950 K for 8 h. Creep test specimens were machined to have a gauge length of 32 mm and a diameter of 6.35 mm along the rolling direction of the plate (ASTM E 139) [14]. Creep test was performed by a constant load in air at 839 to 894 K. The furnaces were equipped with three-zone temperature control units and the temperature difference in a creep specimen was carefully controlled to be less than ± 1 K. The creep strain was measured by high-temperature extensometers. All fitting analysis of creep data was performed using OriginPro 8.6 software. Microstructural observations were made by scanning electron microscopy (SEM) and transmission electron microscopy (TEM) using a FEI Inspect F50 and FEI Tecnai F20, respectively. The initial specimens were mechanically polished down to 1 μm level, and etched by Vilella's reagent (95 mL methanol + 5 mL HCl + 1 g picric acid at room temperature) for the SEM observation. For the phase analysis of the precipitates, X-ray diffraction (XRD) measurement was performed on the powders extracted from the as-tempered specimens and the gauge part of the crept specimens by the anode decomposition method. Electrolyte solution for the anode decomposition was prepared by the mixture of 95 mL methanol + 5 mL HCl. The extracted powders were put into borosilicate capillary tubes to be installed in a Bruker D8 Advance with Cu Kα incident radiation. The step size was 0.02° in two-theta and the counting time was 10 s per step. For the TEM observation, a carbon replica specimen was prepared from the uniformly deformed gauge part of the crept specimen (away from the area of necking to avoid the area of localized deformation). Analyses of the crystallographic structure and

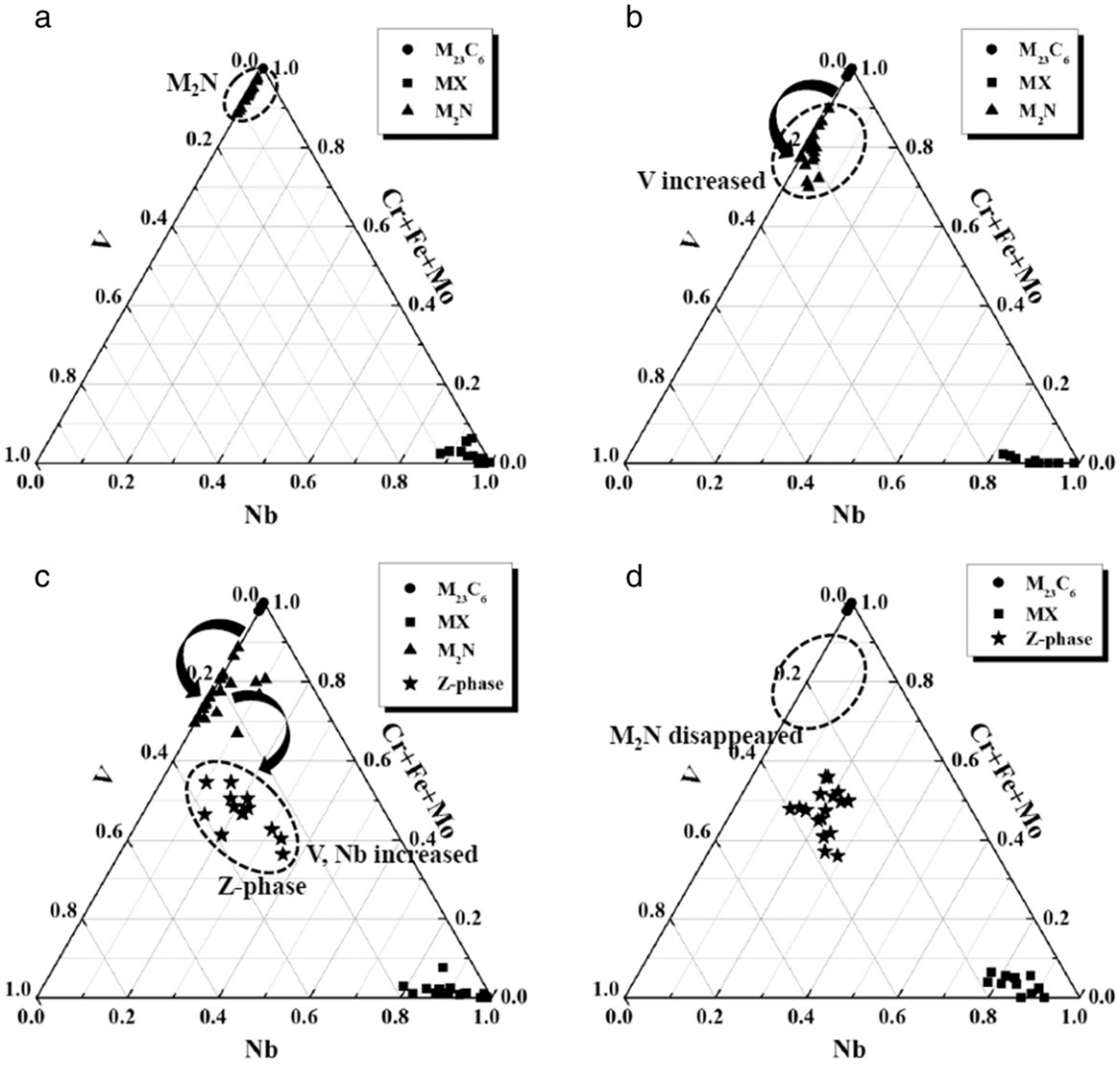

Fig. 6. Ternary diagrams of the metallic composition of the $M_{23}C_6$, MX, M_2N and Z-phase from Steel B. (a) As-tempered, (b) 250 MPa (t_r = 5271 h), (c) 200 MPa (t_r = 7940 h) and (d) 130 MPa (t_r = 17,816 h) at 866 K.

chemical composition of a Z-phase were carried out using selected area electron diffraction (SAED) pattern, energy dispersive spectrum (EDS) and electron energy less spectroscopy (EELS).

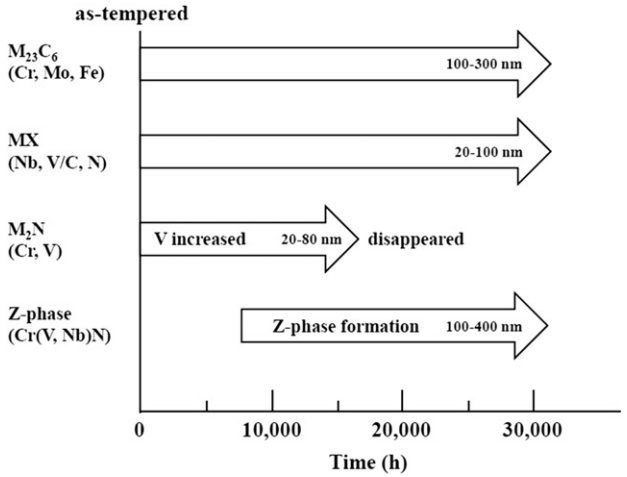

Fig. 7. Precipitation sequence and precipitate size in Steel B at 866 K.

3. Results and discussion

3.1. Initial microstructure

It has been reported that if δ-ferrite is formed on 9–12% Cr martensitic heat-resistant steel, creep strength is considerably degraded at high temperatures [15,16]. Ryu and Yu [16] reported that δ-ferrite was formed if the Cr-equivalence was more than 10. The Cr-equivalence of both steels used in this study was calculated using the Cr-equivalent equation proposed by Ryu and Yu [16], and the result showed that Steel A had 7.75 while Steel B had 8.34, which was expected to have no δ-ferrite formation. These results were also consistent with the microstructural observation using an optical microscope (OM) and SEM, as shown in Fig. 1. The matrix of both steels has a tempered martensite structure, and martensite laths were formed inside PAG boundaries. In addition, fine precipitates were formed on the PAG boundaries and the lath boundaries. To analyze the precipitates, they were collected using anode decomposition, and then XRD analysis was performed (Fig. 2). From the XRD profiles shown in Fig. 2, the fine precipitates shown in Fig. 1 were analyzed to be $M_{23}C_6$ (M = Cr, Fe, Mo), MX and M_2N (M = Cr, V) for both steels. And, for Steel B, which had a high content of Nb, a higher intensity of MX precipitate was observed than Steel A.

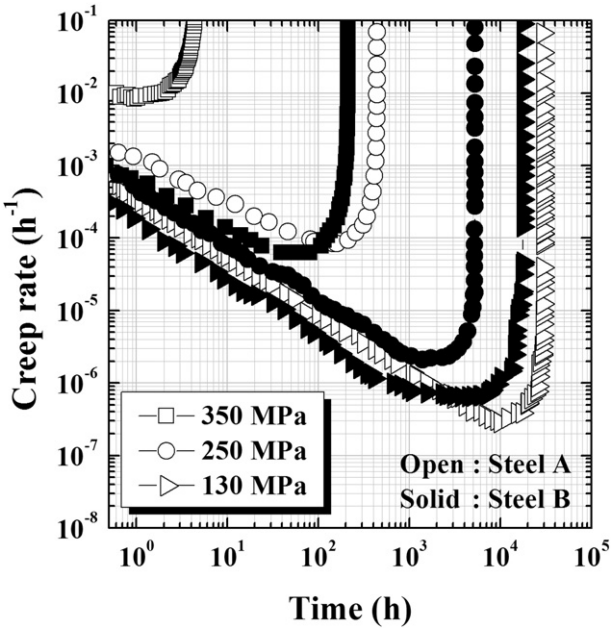

Fig. 8. Creep rate versus time curve at 866 K for Steel A and Steel B.

3.2. Creep-rupture strength

Creep strength is closely related to microstructures such as the types and distributions of precipitates, grain size and dislocation density [1,8]. Fig. 3 shows the creep data of Steel A (black symbol) and Steel B (red symbol) under different stress conditions in a temperature range of 839 to 894 K. The test conditions marked with arrows to the right in this figure indicate that the test is still ongoing. Both steels had increased creep-rupture life for each test temperature as the stress decreased. Nb added Steel B had better creep-rupture strength than Steel A when the applied stress was high (<10,000 h). However, under low stress and long-term test conditions, we had different results. The creep-rupture data of Steel A showed a gradual curve over time as shown in Fig. 3 (black symbol), whereas Steel B showed a rapid reduction in the slope of creep-rupture data from test conditions under 200 MPa at 866 K and 160 MPa at 894 K. In addition, under lower stress conditions than those, the creep-rupture times of both steels became similar and finally they were reversed (a test condition of 866 K with 130 MPa). To analyze the causes of the rapid reduction in creep strength of Steel B over the long-term creep, microstructural analysis was conducted.

3.3. Evolution of microstructure

Fig. 4 shows the results of XRD analysis of the powders extracted from the as-tempered and creep-ruptured specimens of Steel A and Steel B. Fig. 4(a) is the XRD analysis results of Steel A, while Fig. 4(b) shows that of Steel B. As shown in the result of Steel A in Fig. 4(a), no significant change in the major precipitates of Steel A was observed for a long duration time of up to 29,311 h. On the other hand, the results of the creep-ruptured Steel B under 200 MPa, whose creep-rupture strength showed abrupt degradation, verified that the M_2N intensity was reduced and a new peak was formed at 39.6°. In addition, a new peak formed at 39.6°, which increased at the expense of M_2N intensity over time, as shown in the ruptured Steel B at 130 MPa, and the M_2N peak disappeared completely at this test condition. A newly-formed peak for the long-term creep-ruptured specimen of Steel B was analyzed, and the indexing result indicated that it is a Z-phase with a tetragonal structure. Figs. 5 and 6 show the results of

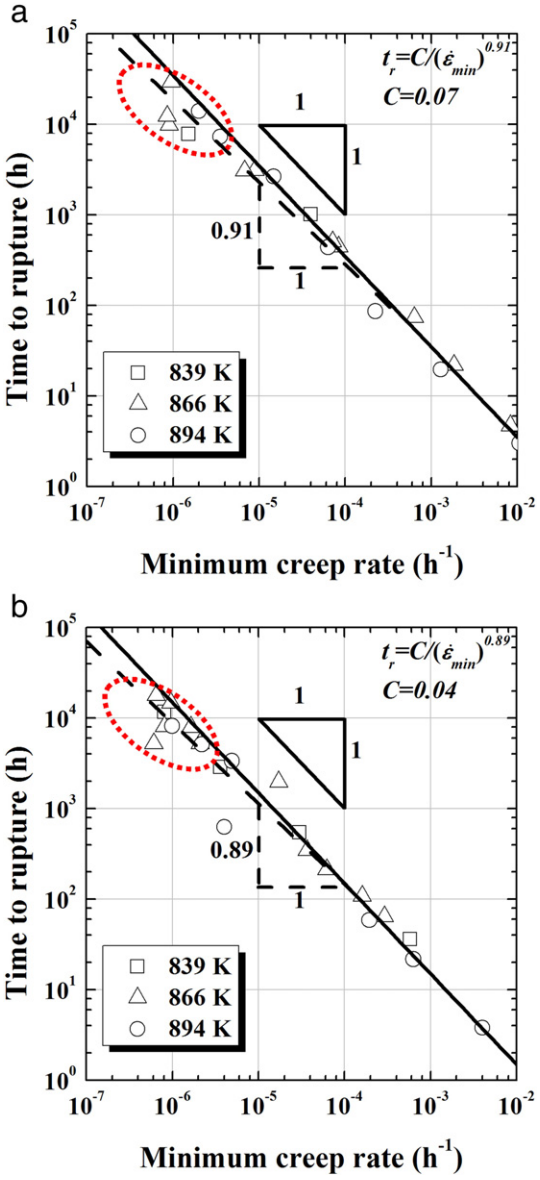

Fig. 9. Relationship between time to rupture and minimum creep rate for (a) Steel A and (b) Steel B.

TEM analysis performed on the specimens prepared by the carbon replica method to do quantitative analysis on the Z-phase. The EDS and SAED pattern also showed that the crystal structure was tetragonal, which is consistent with the XRD analysis shown in Fig. 4(b), and had a Cr(V,Nb)N chemical composition (Fig. 5). Fig. 6 shows the distribution of the metallic compositions of the precipitates marked on ternary compositional diagrams to show the evolution of precipitate-composition during creep deformation. It is noted that the V and Nb content increased in the M_2N precipitates as the creep duration time increased. Also, transition of the M_2N precipitates towards a Z-phase composition appears obvious on the long-term creep test. Precipitation sequence and precipitate size measured in Steel B are summarized in Fig. 7. Precipitation size distribution of over 1000 precipitates per specimen was measured from the TEM images on the carbon replicas. These findings suggest that M_2N precipitates evolved to result in the formation of the Z-phase, which is a thermodynamically stable phase in the creep test temperature. (After 17,816 h at 866 K all M_2N precipitates had disappeared.) It has been reported that the coarsening rate of the Z-phase in 9–12% Cr martensitic heat-resistant steel is significantly high after nucleation, and, as a result, the creep strength was reduced as the solute

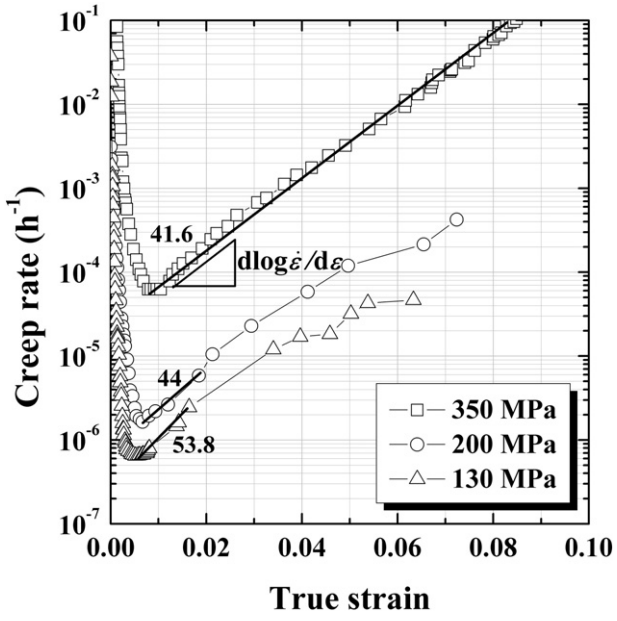

Fig. 10. Creep rate versus strain curves of Steel B at 866 K.

elements such as Cr, V, Nb and N that existed both in the matrix and precipitates were consumed [17–19]. Thus, the reason for the rapid reduction in the creep strength of Steel B (as shown in Fig. 3) was the formation of a Z-phase, mainly by decreasing the precipitation strengthening effect of M_2N nitride.

3.4. Creep-rupture life estimation

Fig. 8 shows the creep strain rate of Steel A and Steel B at 866 K over time. Under high stress and short-term creep conditions, the initial and minimum creep rates of Steel B were lower than those of Steel A by about 1/10, and the creep-rupture strength was superior. This is because the creep strength of Steel B was improved by the Nb addition leading to the enhanced precipitation hardening effect of the Nb-rich MX precipitates observed in Figs. 1 and 2. However, the minimum creep rate of Steel A under 130 MPa where the creep-rupture time was reversed as shown in Fig. 3 was lower than that of Steel B, while Steel B experienced an accelerated creep strain rate into the tertiary creep region after about 7000 h. As shown in the XRD result in Fig. 4, Steel B formed a Z-phase after 7000 h, at which the slope of the creep-rupture time starts rapidly reducing, as shown in Fig. 3. The Monkman–Grant equation [12] explains the relationship between the creep-rupture life and minimum creep rate in the secondary creep region. The equation is as follows:

$$t_r = C_{MG}/(\dot{\varepsilon}_{\min})^m \quad (1)$$

where $\dot{\varepsilon}_{\min}$ is the minimum creep rate, and C_{MG} and m are constants (C_{MG} is the Monkman–Grant constant). The Monkman–Grant equation indicates that the creep-rupture time in each material is inversely proportional to the minimum creep rate ($\dot{\varepsilon}_{\min}$). Most researchers estimate a long-term creep-rupture life based on short-term creep test results using the Monkman–Grant equation [5,20–22]. Fig. 9 shows the Monkman–Grant plot for both Steel A and Steel B. The short-term creep data were relatively well matched to line on the solid lines, but the long-term test results were not: especially the data points for 10,000 h for Steel A and 5000 h for steel B at 866 K deviated from the fitting lines. The constant C_{MG} of Steel A and Steel B was 0.07 and 0.04, while the slope m was 0.91 and 0.89, respectively. F. Abe [13] reported $C_{MG} = 0.025$–1 and $m = 1$ in 2.25Cr–1Mo steel at 723 to 823 K. However, his test result over 873 K showed that the creep-rupture life was

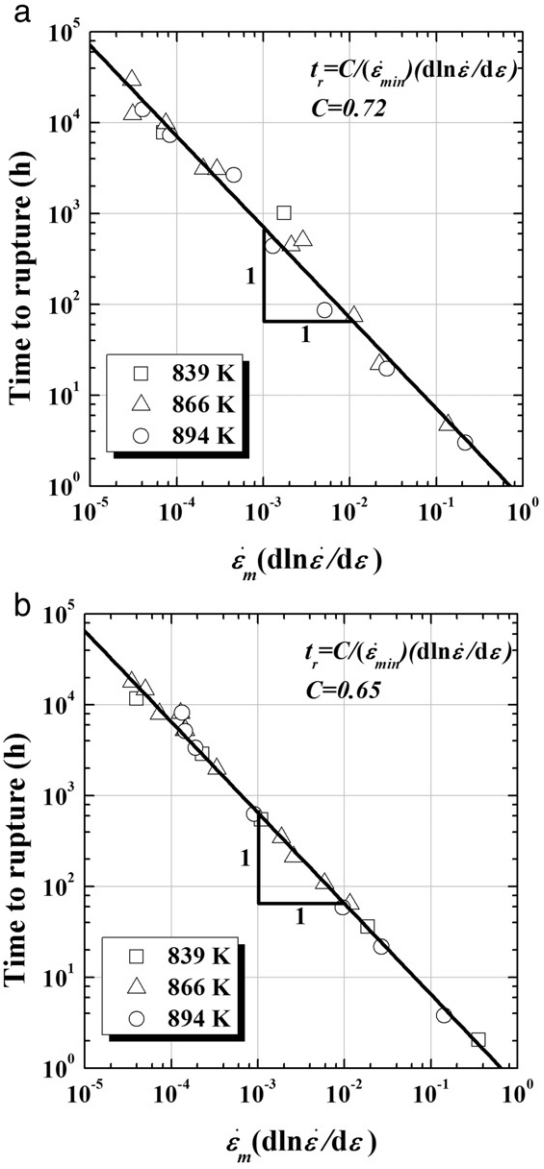

Fig. 11. Relationship between time to rupture and $\dot{\varepsilon}_{\min}(d \ln \dot{\varepsilon}/d\varepsilon)$ given by Eq. (2) for (a) Steel A and (b) Steel B.

significantly short, and exponent m was smaller than 1 ($m < 1$) when compared to the test results under 873 K. These results show errors in the creep-rupture life estimation by the Monkman–Grant equation, in which the slope changes due to changes in the microstructure during long-term creep tests at high-temperature. Prager [23] explained the acceleration creep region using the slope $(d \ln \dot{\varepsilon}/d\varepsilon)$ of the creep rate $(\dot{\varepsilon})$ and the creep strain (ε) curve. The acceleration creep region, the tertiary creep, is a region where the creep strain is accelerated as the creep rate increases after the minimum creep rate. Also, F. Abe [13] proposed the following modified Monkman–Grant Equation by applying the accelerated creep region [23] to the Monkman-Grant equation, Eq. (1):

$$t_r = C_{MMG}/\left[\dot{\varepsilon}_{\min}(d \ln \dot{\varepsilon}/d\varepsilon)\right] \quad (2)$$

where C_{MMG} is the modified Monkman–Grant constant. Fig. 10 shows the $d \ln \dot{\varepsilon}/d\varepsilon$ of Steel B at 866 K. The slope $d \ln \dot{\varepsilon}/d\varepsilon$ of Steel B shows an increasing trend as the stress decreases. That is, with exposure to the long-term creep test temperature, the creep strain was accelerated

due to the formation of a creep void and microstructure degradation. Fig. 11 shows the results of Eq. (2) by applying a creep-rupture time, minimum creep rate and $d \ln \dot{\varepsilon} / d\varepsilon$ for each test condition. The result of the modified Monkman–Grant equation as shown in Fig. 11 showed that the C_{MMG} of Steel A and Steel B was 0.72 and 0.65, while the slopes of both steels were 1. It was verified that the long-term creep-rupture life was well matched when compared with the existing Monkman–Grant equation in Fig. 9. Steel B formed a new Z-phase after about 7000 h at 866 K (Fig. 4), and the creep-rupture time was rapidly reduced after 7000 h (Fig. 3). In addition, the minimum creep rate of Steel B was reached before 7000 h (Fig. 8), so it is not reasonable to apply the Monkman–Grant equation, which can estimate the creep-rupture life using only the minimum creep rate. Thus, this study applied Eq. (2) proposed by F. Abe [13], in which the acceleration creep region was applied, and verified that the observed scattering of a few data points around 5000–10,000 h in the Monkman–Grant plot (Fig. 9) could be improved to make a better fit in the modified Monkman–Grant plot as shown in Fig. 11. Further studies applying the modified Monkman–Grant equation to various other alloys are required.

4. Conclusions

This study evaluated long-term creep characteristics of the high-Cr martensitic high-resistant steels with variation of the Nb-content and studied the validity of a creep-rupture life estimation method. The conclusions of this study are as follows:

1) The major precipitates of both steels after tempering were $M_{23}C_6$, M_2N and MX. Nb-added Steel B showed that M_2N disappeared after about 7000 h at 866 K and a Z-phase formed.
2) Nb-added Steel B showed superior short-term creep strength to that of Steel A whereas the long-term creep strength of Steel A was better than that of Steel B. It was verified that creep strength was rapidly reduced mainly due to the Z-phase formation.
3) Using the Monkman–Grant Equation, the constant C_{MG} of both steels was 0.07 and 0.04, while slope m was 0.91 and 0.89, respectively. In this study, the creep-rupture life estimation equation $\left(t_r = C_{MMG} / \left[\dot{\varepsilon}_{\min} \left(d \ln \dot{\varepsilon} / d\varepsilon\right)\right]\right)$ of the modified Monkman–Grant, in which the accelerated creep region was taken into account, was applied, and constant C_{MMG} in the modified Monkman–Grant equation was 0.72 and 0.65, respectively. When comparing the modified equation with the Monkman–Grant equation, the modified equation revealed results that reasonably matched the estimated and experimental results, although the changes in microstructure occurred due to the long-term creep strain.

Acknowledgments

The authors gratefully acknowledge the financial support provided by the Korea Government Ministry of Knowledge Economy through the Korea Institute of Energy Technology Evaluation and Planning (Grant No. 2012T100201597) and the Korea Institute of Science and Technology (Grant No. 2E25322). The authors also thank Doosan Heavy Industries & Construction Co., Ltd for providing the materials.

References

[1] K.H. Lee, D.B. Park, S.I. Kwun, J.Y. Huh, J.Y. Suh, J.H. Shim, W.S. Jung, Effect of creep deformation on the microstructural evolution of 11CrMoVNb heat resistant steel, Mater. Sci. Eng. A 536 (2012) 92–97.
[2] K. Sawada, T. Hara, M. Tabuchi, K. Kimura, K. Kubushiro, Microstructure characterization of heat affected zone after welding in Mod.9Cr–1Mo steel, Mater. Charact. 101 (2015) 106–113.
[3] K. Kimura, S. Yamaoka, Influence of high pressure normalizing heat treatment on microstructure and creep strength of high Cr steels, Mater. Sci. Eng. A 387 (2004) 628–632.
[4] F. Abe, Precipitate design for creep strengthening of 9% Cr tempered martensitic steel for ultra-supercritical power plants, Sci. Technol. Adv. Mater. 9 (2008) 1–15.
[5] K. Kimura, H. Kushima, K. Sawada, Long-term creep deformation property of modified 9Cr–1Mo steel, Mater. Sci. Eng. A 510–1 (2009) 58–63.
[6] K. Sawada, M. Tabuchi, H. Hongo, T. Watanabe, K. Kimura, Z-phase formation in welded joints of high chromium ferritic steels after long-term creep, Mater. Charact. 59 (2008) 1161–1167.
[7] W. Bendick, L. Cipolla, J. Gabrel, J. Hald, New ECCC assessment of creep rupture strength for steel grade X10CrMoVNb9-1 (Grade 91), Int. J. Press. Vessel. Pip. 87 (2010) 304–309.
[8] M. Taneike, F. Abe, K. Sawada, Creep-strengthening of steel at high temperatures using nano-sized carbonitride dispersions, Nature 424 (2003) 294–296.
[9] ASME Boiler and Pressure Vessel Code; Section II, Materials, 2011. 839–840.
[10] F.R. Larson, J. Miller, A time–temperature relationship for rupture and creep stress, Trans. ASME 74 (1952) 765–775.
[11] M. Tamura, F. Abe, K. Shiba, H. Sakasegawa, H. Tanigawa, Larson–Miller constant of heat-resistant steel, Metall. Mater. Trans. A 44 (2013) 2645–2661.
[12] F.C. Monkman, N.J. Grant, An empirical relationship between rupture life and minimum creep rate in creep-rupture tests, Proc. ASTM 56 (1956) 593–620.
[13] F. Abe, Stress to produce a minimum creep rate of 10^{-5}%/h and stress to cause rupture at 10^5 h for ferritic and austenitic steels and superalloys, Int. J. Press. Vessel. Pip. 85 (2008) 99–107.
[14] ASTM E 139-11, Standard test methods for conducting creep, creep-rupture, and stress-rupture tests of metallic materials (2011).
[15] M. Yoshizawa, M. Igarashi, Long-term creep deformation characteristics of advanced ferritic steels for **USC** power plants, Int. J. Press. Vessel. Pip. 84 (2007) 37–43.
[16] S.H. Ryu, Jin Yu, A new equation for the Cr equivalent in 9 to 12 pct Cr steels, Metall. Mater. Trans. A 29 (1998) 1573–1578.
[17] K. Sawada, K. Suzuki, H. Kushima, M. Tabuchi, K. Kimura, Effect of tempering temperature on Z-phase formation and creep strength in 9Cr–1Mo–V–Nb–N steel, Mater. Sci. Eng. A 480 (2008) 558–563.
[18] H.K. Danielsen, J. Hald, On the nucleation and dissolution process of Z-phase Cr(V, Nb)N in martensitic 12%Cr steels, Mater. Sci. Eng. A 505 (2009) 169–177.
[19] M. Yoshizawa, M. Igarashi, K. Moriguchi, A. Iseda, H.G. Armaki, K. Maruyama, Effect of precipitates on long-term creep deformation properties of P92 and P122 type advanced ferritic steels for USC power plants, Mater. Sci. Eng. A 510–1 (2009) 162–168.
[20] B.K. Choudhary, E.I. Samuel, Creep behavior of modified 9Cr–1Mo ferritic steel, J. Nucl. Mater. 412 (2011) 82–89.
[21] E.I. Samuel, B.K. Choudhary, D.P.R. Palaparti, M.D. Mathew, Creep deformation and rupture behavior of P92 steel at 923 K, Procedia Eng. 55 (2013) 64–69.
[22] H.O. Ali, M.N. Tamin, Modified Monkman–Grant relationship for austenitic stainless steel foils, J. Nucl. Mater. 433 (2013) 74–79.
[23] M. Prager, Development of the MPC omega method for life assessment in the creep range, J. Press. Vessel. Technol. 117 (1995) 95–103.